Dalton Transactions

Dicationic ionic liquids with the difluorophosphate anion

Journal:	*Dalton Transactions*
Manuscript ID	DT-ART-04-2025-000930.R1
Article Type:	Paper
Date Submitted by the Author:	15-May-2025

Complete List of Authors:	Kamada, Kentarou; Kyoto University, Graduate School of Energy Science Nishimoto, Kohei; Kyoto University, Graduate School of Energy Science Nokami, Toshiki; Tottori University - Tottori Campus, Chemistry and Biotechnology Nakajima, Hideto; Kyoto University, Graduate School of Engineering Hwang, Jinkwang; Kyoto University, Graduate School of Energy Science Matsumoto, Kazuhiko; Kyoto University, Graduate School of Energy Science

Dicationic ionic liquids with the difluorophosphate anion

Kentaro Kamada,[a] Kohei Nishimoto,[a] Toshiki Nokami,[b] Hideto Nakajima,[c] Jinkwang Hwang,[a] Kazuhiko Matsumoto[a,*]

[a]Graduate School of Energy Science, Kyoto University, Yoshida-honmachi, Sakyo-ku, Kyoto 606-8501, Japan.

[b]Faculty of Engineering, Tottori University, 4-101, Koyama-cho minami, Tottori, Japan.

[c]Graduate School of Engineering, Kyoto University, Kyotodaigakukatsura, Nishikyo-ku, Kyoto 615-8510, Japan

*Corresponding authors: Kazuhiko Matsumoto

E-mail: matsumoto.kazuhiko.4c@kyoto-u.ac.jp (K.M.)

Tel: +81757535827

Fax: +81757535906

†Electronic supplementary information (ESI) available. See DOI: https://doi.org/xx.xxxx/xxxxxxxx.

Abstract

Dicationic ionic liquids can be diversely designed by tuning the spacer and cationic center structures. Their potentially superior features compared to conventional ionic liquids include enhanced thermal stability and wide potential window, making them promising candidates as electrolytes for secondary batteries. However, there are relatively few reports on dicationic ionic liquids, and the relationship between their structure and physical properties remains largely unexplored. In this study, a series of dicationic ionic liquids are synthesized combined with $PO_2F_2^-$. The effects of cationic, anionic, and linker structures on their physical and electrochemical properties are discussed through different analytical and computational methods. The cationic structures examined include pyrrolidinium, ammonium, and imidazolium, while the anionic impact was pursued by comparing the case with BF_4^-. The dicationic ionic liquid with an ether linker emerged as a promising case due to its high ionic conductivity and wide electrochemical window among all the tested salts.

Introduction

Ionic liquids (ILs), solely composed of ionic species, are known for their low volatility, low flammability, chemical and physical stabilities, wide electrochemical window, ease of separation, and high solubility for certain compounds.[1-4] These properties make ILs particularly suitable for use as electrolytes, owing to their high ionic conductivity and thermal stability.[5-9] Among the cations incorporated in ILs, pyrrolidinium and imidazolium are the most widely studied in diverse topics. The pyrrolidinium cation is notable for its high electrochemical and thermal stabilities, making it suitable for a variety of applications.[10, 11] In contrast, the imidazolium cation exhibits low viscosity due to its aromaticity which results in electron delocalization and weak interactions with anions.[12]

In recent years, the synthesis, properties, and applications of dicationic ionic liquids (DILs) have been reported in various studies.[13] DILs consist of a doubly charged cation, typically two positively charged groups such as ammonium moieties being connected by a linker, and two anions. They can be further classified into symmetric DILs with two identical positively charged groups at both the ends and asymmetric DILs with two different ones. The asymmetric structure sometimes induces different physical properties from those of symmetric structures; for example, Armstrong et al. reported that asymmetric DILs, such as $[(P_{333})C_5(N_{111})][TFSA]_2$ ($(P_{333})C_5(N_{111})^+$ = (1-trimehtylammonium-yl-pentyl)-tripropylphosphonium) and $TFSA^-$ = (bis(trifluoromethylsulfonyl)amide), exhibit lower melting points than those of the symmetric DILs.[14] While asymmetric DILs offer the potential to discover novel properties, they are challenging to synthesize in high purity or to purify to high standards, making symmetric DILs more suitable when facile synthesis and high purity are required.[11]

The DILs exhibit some superior properties compared to monocationic ILs, such as high

thermal stability, wide electrochemical stabilities, and low toxicity.[15, 16] These features make them promising candidates for applications in electrochemical applications, stationary phases in gas chromatography, reaction catalysts, lubricants, and as non-toxic or antimicrobial materials.[17-21] In particular, imidazolium-based DILs were synthesized and evaluated as electrolytes for lithium-ion batteries, showing improved cycle performance compared to monocationic ILs.[17]

However, DILs also have some drawbacks, particularly related to their large molecular size and double charge, which raises the cation-anion interaction, increasing viscosity and melting points and subsequently decreasing the ionic conductivity. These factors, viscosity and melting point, are critical for determining the feasibility of DILs for specific applications. The synthesis and physical properties of pyrrolidinium-based DILs have been previously investigated. For instance, focusing on the linker length, the melting point of $[C_3\text{-}(C_1pyrr)_2][TFSA]_2$ ($C_3\text{-}(C_1pyrr)_2^+$ = (1,3-bis(1-methylpyrrolidinium-1-yl)propane) with the propyl linker was reported to be 206 °C.[22] While, the melting point decreases with elongating the linker to hexyl and decyl groups; $[C_6\text{-}(C_1pyrr)_2][TFSA]_2$ ($C_6\text{-}(C_1pyrr)_2^+$ = (1,6-bis(1-methylpyrrolidinium-1-yl)hexane) has a melting point of 64–66°C, and $[C_{10}\text{-}(C_1pyrr)_2][TFSA]_2$ ($C_{10}\text{-}(C_1pyrr)_2^+$ = (1,10-bis(1-methylpyrrolidinium-1-yl)decane) is liquid at room temperature.[23] Although increasing the linker length decreases the melting point, it tends to increase the viscosity.

Concerning viscosity, previous studies on monocationic ILs revealed that the length and modification of the side-chain significantly affect the viscosity. While the elongation of an alkyl chain simply leads to an increase of the viscosity,[24] the introduction of oxygen atoms into the side chain reduces the viscosity compared to purely carbon-based linkers. For example, [*N*-hexyl-*N*-methylpiperidinium][TFSA] has a viscosity of 266 mPa s, and oxygen substitutions at

the β or γ positions of the hexyl chain, i.e. methoxy-ethoxy-methyl (MEM or C_{1O2O1}), reduce the viscosity to 89 mPa s.[25]

Choice of anionic species for ILs is limited compared to cationic species. Fluorocomplex anions, PF_6^- and BF_4^-, are widely employed for ILs due to their weak interaction with cations, attributed to the charge delocalization based on multiple fluorine atoms surrounding the central atom.[26] Simple synthetic routes to these anions are attractive for practical use in IL production. However, their hydrolytic instability can generate toxic and corrosive species, including HF. The $PO_2F_2^-$ anion, which can be regarded as a species obtained by substituting four fluorine atoms in PF_6^- with two oxygen atoms and a hydrolytic decomposition product of PF_6^-, is a safer alternative with greater hydrolysis resistance compared to PF_6^-.[26] Metal $PO_2F_2^-$ salts generally exhibit low solubilities, being not suitable as a main salt in electrolytic solutions. On the other hand, metal $PO_2F_2^-$ salt is extensively recognized as a promising additive for lithium, sodium and potassium ion batteries in academic and industrial levels.[27-32] The $PO_2F_2^-$ anion was also used for ILs combined with some organic cations.[26] The large dipole moment and low symmetry of $PO_2F_2^-$ (C_{2v}) differentiate it from nonpolar PF_6^- (O_h) and BF_4^- (T_d). The melting point of $[C_2C_1im][PO_2F_2]$ ($C_2C_1im^+$ = 1-ethyl-3-methylimidazolium) is slightly lower than the corresponding PF_6^- and BF_4^- salts, and its viscosity is close to that of $[C_2C_1im][BF_4]$. Solvatochromic analysis identified the pronounced donor property of $PO_2F_2^-$ in $[C_2C_1im][PO_2F_2]$ compared to PF_6^- and BF_4^- anions in their corresponding $C_2C_1im^+$ ILs.

Although some $PO_2F_2^-$ ILs are known, they have not been extensively explored for a variety of cations. In this study, we synthesized DILs composed of dications with an ether linker and $PO_2F_2^-$ and evaluated their physical and electrochemical properties by elucidating the effects of linker, cationic, and anionic structures.

Result and discussion

Synthesis. The synthesis of dicationic salts with an ether linker was completed in three steps (**Scheme 1**). In the first step, 1,2-bis(chloromethoxy)ethane was synthesized by reacting ethylene glycol with paraformaldehyde and trimethylchlorosilane in dichloromethane.[25] In the second step, the resulting 1,2-bis(chloromethoxy)ethane was reacted with the corresponding amine in dichloromethane. Finally, the target dicationic salts were obtained by ion exchange between the chloride salt and $K[PO_2F_2]$ or $K[BF_4]$ in acetone. The quarternization and ion exchange reactions proceed in high yields, whereas the yield of 1,2-bis(chloromethoxy)ethane was typically below 50 %. For the synthesis of DILs with an alkyl-chain linker, 1-methylpyrrolidine was reacted with 1,6-dichlorohexane in acetonitrile, followed by ion exchange with $K[PO_2F_2]$ (**Scheme 2**). The resulting $PO_2F_2^-$ salts are all characterized by triplet signals around −16.0 ppm and doublet signals around −80.6 ppm in ^{31}P and ^{19}F nuclear magnetic resonance (NMR) spectra, respectively, and absorption bands around 500, 800, 1130, and 1310 cm^{-1} in infrared (IR) spectra (see the Experimental section for the detailed spectroscopic data). **Figure 1** illustrates the five dicationic compounds synthesized in this study. The cationic moieties are methylpyrrolidinium, diethylmethylammonium, and methylimidazolium, and the anions are $PO_2F_2^-$ and BF_4^-.

Computational results. The structures of the dications and anions considered in this study were optimized by DFT calculations at PBE1PBE/aug-cc-pVDZ and resulted in stationary points with all frequencies being real. Related monocations, which were obtained by cutting the dications into halves at the center of the linker chain, were also calculated in the same way for comparison (see **Figure S1** for the 12 cationic species considered in this work and **Supplementary Information** for the atomic coordinates of the calculated dicationic, anionic,

and monocationic species). The optimized geometries with electrostatic potential maps for C_{1O2O1}-$(C_1pyrr)_2^{2+}$ (C_{1O2O1}-$(C_1pyrr)_2^{2+}$ = (1,6-bis(1-methylpyrrolidinium-1-yl)methoxy-ethoxy-ethane) and C_6-$(C_1pyrr)_2^{2+}$ are shown in **Figure 2**. All the structures reach the linker chains with trans conformers under optimized conditions regardless of the ammonium structure and presence of oxygen atoms. Electrostatic potential mapping clearly demonstrates the negative charge on the oxygen atom in the ether linker of C_{1O2O1}-$(C_1pyrr)_2^{2+}$. Other negatively charged parts are observed around the hydrogen atoms at the C3 and C4 carbon atoms in the pyrrolidinium rings. The positive charge around the nitrogen atom in the pyrrolidinium ring also increases upon incorporation of the ether chain, which may cause the lower cathodic stability of the cation with the ether chain (see below). Details on electrochemical stabilities of the ionic species will be discussed later in the section of electrochemical properties.

Thermal properties. The thermal and physical properties of the dicationic salts prepared in this work are summarized in **Table 1** (thermal transition temperature and density, viscosity, and ionic conductivity, and electrochemical windows). The thermal properties were analyzed by differential scanning calorimetry (DSC) under an argon atmosphere at a heating rate of 5 K min^{-1}. According to the DSC analysis, $[C_6$-$(C_1pyrr)_2][PO_2F_2]_2$ and $[C_{1O2O1}$-$(C_1im)_2][PO_2F_2]_2$ (C_{1O2O1}-$(C_1im)_2^{2+}$ = (1,6-bis(1-methylimidazolium-1-yl)methoxy-ethoxy-methane), are solid at room temperature and have melting points above 373 K (**Figure S2**). On the other hand, no crystallization is observed for $[C_{1O2O1}$-$(C_1pyrr)_2][PO_2F_2]_2$, $[C_{1O2O1}$-$(C_1pyrr)_2][BF_4]_2$, and $[C_{1O2O1}$-$(N_{221})_2][PO_2F_2]_2$ (C_{1O2O1}-$(N_{221})_2^{2+}$ = (1,6-bis(*N*,*N*-diethylmethylammonium-1-yl)methoxy-ethoxy-methane), where they only exhibit glass transition and keep the liquid state at room temperature (**Figure 3**). Although the contrast of the surface charge varies by introducing the ether linker (C_{1O2O1}-$(C_1pyrr)_2^+$ exhibits more localized positive and negative charges than C_6-$(C_1pyrr)_2^+$, Figure 2), the lower freedom of the alkyl chain seems to make a

more significant impact on crystallization (C_6 vs. C_{1O2O1} in the linker). Comparing the three PO_2F_2 salts with the ether linker, the different crystallization behavior for $[C_{1O2O1}\text{-}(C_1im)_2][PO_2F_2]_2$ can be attributed to the imidazolium ring structure that forms intermolecular π-π stacking interaction between aromatic rings and facilitates crystallization.[22, 33] The glass transition temperature follows the trend of 200 K for $[C_{1O2O1}\text{-}(C_1pyrr)_2][PO_2F_2]_2$, 205 K for $[C_{1O2O1}\text{-}(N_{221})_2][PO_2F_2]_2$, and 224 K for $[C_{1O2O1}\text{-}(C_1pyrr)_2][BF_4]_2$, stressing the higher fluidity of $PO_2F_2^-$-based DILs compared to BF_4^--based DILs (see the viscosity data below) by considering the correlation between glass transition temperature and viscosity. It should be noted that the high viscosities of the present dicationic salts could kinetically prevent crystallization and conceal the crystallization behavior under the present DSC conditions.[34] In previous studies, the glass transition temperatures of dicationic salts with imidazolium structures, such as $[C_{2O2}\text{-}(C_1im)_2][TFSA]_2$ and $[C_{2O2O2}\text{-}(C_1im)_2][TFSA]_2$ ($C_{2O2}\text{-}(C_1im)_2^{2+}$ = (1,5-bis(1-methylimidazolium-1-yl)ethoxy-ethane) and $C_{2O2O2}\text{-}(C_1im)_2^{2+}$ = (1,8-bis(1-methylimidazolium-1-yl)ethoxy-ethoxy-ethane), were found to be lower than those of the corresponding dicationic salts without an ether linker.[22, 33] Similarly, in pyrrolidinium structures, introduction of an ether chain linker decreased the melting point or T_g.[35]

Physical properties. In the following section on physical properties, the three DILs, which are liquid at room temperature ($[C_{1O2O1}\text{-}(C_1pyrr)_2][PO_2F_2]_2$, $[C_{1O2O1}\text{-}(N_{221})_2][PO_2F_2]_2$ and $[C_{1O2O1}\text{-}(C_1pyrr)_2][BF_4]_2$) are discussed. The temperature dependence of the densities of the DILs is shown in **Figure 4a** (see **Table S1** for the density data). The density linearly decreased with increasing temperature, following Equation (1).

$$\rho = AT + B \quad (1)$$

where ρ and T denote the density and temperature, respectively, and A and B are the fitting parameters determined by mathematical fitting (see **Table S1** for these fitting parameters). Among the three compounds, $[C_{1O2O1}\text{-}(C_1pyrr)_2][PO_2F_2]_2$ exhibits the highest density. As stated in the following discussion, density is a parameter related to both cation and anion. Although the carbon numbers of the cations are the same for $[C_{1O2O1}\text{-}(C_1pyrr)_2][PO_2F_2]_2$ and $[C_{1O2O1}\text{-}(N_{221})_2][PO_2F_2]_2$, $C_{1O2O1}\text{-}(N_{221})_2^{2+}$ with a linear alkyl chain has a higher flexibility than $C_{1O2O1}\text{-}(C_1pyrr)_2^{2+}$ with a restricted cyclic structure, which results in the higher molecular motion and thus lower density of the former than those of the latter (1.349 g cm^{-3} for $[C_{1O2O1}\text{-}(C_1pyrr)_2][PO_2F_2]_2$ and 1.277 g cm^{-3} for $[C_{1O2O1}\text{-}(N_{221})_2][PO_2F_2]_2$ at 298 K). Because $PO_2F_2^-$ is heavier than BF_4^- and their difference in volume cannot compensate it, $PO_2F_2^-$ salts exhibit higher densities than BF_4^- salts (e.g. 1.23 g cm^{-3} for $[N_{2222}][PO_2F_2]$ and 1.21 g cm^{-3} for $[N_{2222}][BF_4]$ at 298 K, where N_{2222}^+ = tetraethylammonium cation). [36] This is also the case for the present two salts, $[C_{1O2O1}\text{-}(C_1pyrr)_2][PO_2F_2]_2$ and $[C_{1O2O1}\text{-}(C_1pyrr)_2][BF_4]_2$ (1.349 g cm^{-3} for $[C_{1O2O1}\text{-}(C_1pyrr)_2][PO_2F_2]_2$ and 1.305 g cm^{-3}for $[C_{1O2O1}\text{-}(C_1pyrr)_2][BF_4]_2$ at 298 K).

The temperature dependence of the viscosities for $[C_{1O2O1}\text{-}(C_1pyrr)_2][PO_2F_2]_2$, $[C_{1O2O1}\text{-}(N_{221})_2][PO_2F_2]_2$, and $[C_{1O2O1}\text{-}(C_1pyrr)_2][BF_4]_2$ are shown in **Figure 4b** (see **Table S2** for the viscosity data). Viscosities were measured over a temperature range of 278 K to 338 K at 10 K intervals, and the resulting data were fitted with the Vogel-Tammann-Fulcher (VTF) equation (**Equation (2)**).[37-39]

$$\eta\,(\mathrm{T}) = \mathrm{A}_{\eta}\sqrt{\mathrm{T}}\exp\left(\frac{\mathrm{B}_{\eta}}{T-\mathrm{T}_{0\,\eta}}\right) \qquad (2)$$

where η denotes viscosity and A_η, B_η, and $T_{0\eta}$ are fitting parameters determined by mathematical fitting (see **Table S2** for these fitting parameters).

Such a behavior as fragile liquids were known for various ILs in previous reports.[40-42] The lower viscosity of $[C_{1O2O1}\text{-}(C_1pyrr)_2][PO_2F_2]_2$ (2000 mPa s) than $[C_{1O2O1}\text{-}(N_{221})_2][PO_2F_2]_2$ (3700 mPa s) agrees with the previously reported trend between the pyrrolidinium-based and ammonium-based ILs with the common anion (e.g. 57.6 mPa s for $[C_{2O1}C_1pyrr][TFSA]$ vs. 70 mPa s for $[C_{2O1}N_{221}][TFSA]$; 36.5 mPa s for $[C_{2O1}C_1pyrr)_2][FSA]$ vs. 49 mPa s for $[C_{2O1}N_{221}][FSA]$, where $C_{2O1}C_1pyrr^+$ = *N*-methyl-*N*-methoxyethylpyrrolidinium and $C_{2O1}N_{221}^+$ = *N*,*N*-Diethyl-*N*-methyl-*N*-(2-methoxyethyl)ammonium).[43, 44] Contrary to the previous findings with fluorocomplex anions in monocationic ILs,[26] $[C_{1O2O1}\text{-}(C_1pyrr)_2][PO_2F_2]_2$ exhibits a lower viscosity than that of $[C_{1O2O1}\text{-}(C_1pyrr)_2][BF_4]_2$ (2000 mPa s for $[C_{1O2O1}\text{-}(C_1pyrr)_2][PO_2F_2]_2$ and 11900 mPa s for $[C_{1O2O1}\text{-}(C_1pyrr)_2][BF_4]_2$ at 298 K). This trend can be attributed to the large and doubly charged cations of DILs, where both the van der Waals interaction of cations and electrostatic cation-anion interaction mainly dominate the viscosity. The former is common in the two DILs, whereas the latter is affected by the characteristics of the anions. The larger $PO_2F_2^-$ anion is intrinsically beneficial than BF_4^- in terms of electrostatic interaction, but the large dipole moment on $PO_2F_2^-$ can also affect such local interactions. Compared to alkylimidazolium cations, alkylpyrroridinium cation has a lower positive charge concentration due to the absence of aromatic hydrogen atoms. Consequently, the balance of several factors seems to lead to the lower viscosity of the $PO_2F_2^-$-based DIL than that of the BF_4^--based DIL. Glass transition temperature has a significant correlation with viscosity; a substance with a low glass transition temperature tends to exhibit a low viscosity. The lower glass transition temperature of $[C_{1O2O1}\text{-}(C_1pyrr)_2][PO_2F_2]_2$ (Figure 3) also correlates with its lower viscosity than $[C_{1O2O1}\text{-}(C_1pyrr)_2][BF_4]_2$.

The ionic conductivities, shown in **Figure 4c** (see **Table S3** for the ionic conductivity data), followed an opposite trend to viscosities, while higher ionic conductivity values observed for

lower viscosity compounds. The ionic conductivity was also analyzed using the VTF equation (**Equation (3)**).

$$\sigma\ (\mathrm{T}) = \frac{\mathrm{A}_\sigma}{\sqrt{\mathrm{T}}}\exp\left(-\frac{\mathrm{B}_\sigma}{T-\mathrm{T}_{0\,\sigma}}\right) \qquad (3)$$

where σ denotes ionic conductivity and A_σ, B_σ, and $T_{0\sigma}$ are fitting parameters determined by mathematical fitting (see **Table S3** for these fitting parameters). Although the observed ionic conductivities (0.425, 0.222, and 0.132 mS cm^{-1} at 298 K for $[C_{1O2O1}\text{-}(C_1pyrr)_2][PO_2F_2]_2$, $[C_{1O2O1}\text{-}(N_{221})_2][PO_2F_2]_2$, and $[C_{1O2O1}\text{-}(C_1pyrr)_2][BF_4]_2$) are lower than typical ILs of fluorocomplex anions (12 mS cm^{-1} at 298 K for $[C_2C_1im][PO_2F_2]$, 3.6 mS cm^{-1} at 308 K for $[C_4C_1pyrr][PO_2F_2]$ ($C_4C_1pyrr^+$ = *N*-butyl-*N*-methylpyrrolidinium), and 14 mS cm^{-1} at 298 K for $[C_2C_1im][BF_4]$)[26, 45] by one order or more, they are comparable to the values of known DILs (0.78 mS cm^{-1} at 298 K for $[C_{2O2O2}\text{-}(C_1pyrr)_2][TFSA]_2$ (1,8-bis(1-methylpyrrolidinium-1-yl)ethoxy-ethoxy-ethane)).[35] The higher viscosity and molar volume (thus lower number of ions per volume) of $C_{1O2O1}\text{-}(N_{221})_2^{2+}$ than $C_{1O2O1}\text{-}(C_1pyrr)_2^{2+}$ can account for the difference of ionic conductivities between $[C_{1O2O1}\text{-}(C_1pyrr)_2][PO_2F_2]_2$ and $[C_{1O2O1}\text{-}(N_{221})_2][PO_2F_2]_2$ through the Walden rule (see **Tables S4 and S5** and **Figure S3** for molar concentration, molar ionic conductivity, and Walden plot).[40, 46, 47] Viscosity can also rationalize the higher ionic conductivity of $[C_{1O2O1}\text{-}(C_1pyrr)_2][PO_2F_2]_2$ than that of $[C_{1O2O1}\text{-}(C_1pyrr)_2][BF_4]_2$.

Electrochemical properties. The electrochemical stabilities of $[C_{1O2O1}\text{-}(C_1pyrr)_2][PO_2F_2]_2$, $[C_{1O2O1}\text{-}(N_{221})_2][PO_2F_2]_2$ and $[C_{1O2O1}\text{-}(C_1pyrr)_2][BF_4]_2$ were evaluated by cyclic voltammetry with a three-electrode cell. The cyclic voltammograms of a glass-like carbon electrode in the three DILs are shown in **Figure 5**. Under the threshold of 0.1 mA cm^{-2}, the anodic limit is 1.90 V for both $[C_{1O2O1}\text{-}(C_1pyrr)_2][PO_2F_2]_2$ and $[C_{1O2O1}\text{-}(N_{221})_2][PO_2F_2]_2$. The anodic limit of 2.80

V for $[C_{1O2O1}\text{-}(C_1pyrr)_2][BF_4]_2$ is higher than that of $[C_{1O2O1}\text{-}(C_1pyrr)_2][PO_2F_2]_2$. Although this trend is consistent with previous reports on monocationic ILs,[48] the anodic limits of the DILs are higher than those of monocationic ILs such as $[C_2C_1im][PO_2F_2]$ and $[C_2C_1im][BF_4]$ by 0.5 V.[48] A similar trend was also reported for $[C_6\text{-}(C_1im)_2][TFSA]_2$ and $[C_6C_1im][TFSA]$ ($C_6\text{-}(C_1im)_2^+$ = 1,6-bis(1-methylimidazolium-1-yl)hexane and $C_6C_1im^+$ =1-hexyl-3-methylimidazolium).[17, 49] Discussion on the cathodic limit is somewhat vague due to the appearance of multiple cathodic waves. Such behavior sometimes occurs even in ILs containing very high concentration of ions, but not for typical monocationic quaternary ammonium-based ILs combined with inorganic fluorocomplex anions.[45] Although the formation of an inactive surface film based on the reductive decomposition of the dications is possible, further work is required to clarify this point. Nevertheless, the same criterion as the anodic limit leads to the cathodic limits of −3.01 V for $[C_{1O2O1}\text{-}(C_1pyrr)_2][PO_2F_2]_2$, −2.37 V for $[C_{1O2O1}\text{-}(N_{221})_2][PO_2F_2]_2$, and −2.11 V for $[C_{1O2O1}\text{-}(C_1pyrr)_2][BF_4]_2$.

The stabilities of the dications, monocations, and anions against reduction and oxidation were evaluated by explicitly taking the difference between the energy of an ion and the energy of that ion with one more or one less electron in DFT calculations. The resulting electrochemical stabilities using the polarizable continuum model (PCM) with a dielectric constant of 15.0 are summarized in **Figure 6**. Calculation under vacuum provides an extreme trend; the cathodic and anodic limits are determined by cation and anion, respectively (**Figure S4**) as pointed out in a previous work.[50] On the other hand, application of the PCM, in a general sense, translates the limits of the cations and anions to the lower and higher potentials, respectively. Although the PCM calculations are prone to overestimate the electrochemical windows of ILs,[50] the overall trend can be discussed by comparing them.

Imidazolium-based cations are less stable both anodically and cathodically than

pyrrolidinium- and ammonium-based cations. Although dications are less stable against reduction and more stable against oxidation compared to the corresponding monocations under vacuum (i.e. C_{1O2O1}-$(C_1pyrr)_2^{2+}$ vs. $C_3C_1pyrr^+$) probably due to the double positive charge on dications, it is less evident in the PCM calculations. Effects of the ether group in the linker or side-chain is slightly complicated. The ether group in the linker or side-chain diminishes the reductive stability of the cation compared to the one with the corresponding alkyl group in any cationic frame (e.g. C_{1O2O1}-$(C_1pyrr)_2^{2+}$ vs. $C_6(C_1pyrr)_2^+$). On the other hand, the oxidative stabilities of the imidazolium series do not change by incorporating an ether group, which is in contrast to the distinct difference of oxidative stability between the pyrrolidinium cations with ether and alkyl groups (or the ammonium cations as well). The HOMO and LUMO diagrams of C_{1O2O1}-$(C_1pyrr)_2^{2+}$, C_6-$(C_1pyrr)_2^{2+}$, $C_{1O1}C_1pyrr^+$ (C_{1O1}-C_1pyrr^+ = (*N*-methyl-*N*-methoxymethylpyrrolidinium), and $C_3C_1pyrr^+$ ($C_3C_1pyrr^+$ = (*N*-methyl-*N*-propylpyrrolidinium) are shown in **Figure 7**. The shape of HOMO is not very sensitive to the charge on the cation; C_{1O2O1}-$(C_1pyrr)_2^{2+}$ and $C_{1O1}C_1pyrr^+$ give similar HOMO diagrams (C_6-$(C_1pyrr)_2^{2+}$ and $C_3C_1pyrr^+$ as well). The HOMO of C_6-$(C_1pyrr)_2^{2+}$ is slightly different from that of C_{1O2O1}-$(C_1pyrr)_2^{2+}$, and introduction of oxygen atoms affects the symmetry of HOMO. Effects of dication formation is more distinct in LUMO. Both the C_{1O2O1}-$(C_1pyrr)_2^{2+}$ and C_6-$(C_1pyrr)_2^{2+}$ dications have LUMO on the linker, whereas the $C_{1O1}C_1pyrr^+$ and $C_3C_1pyrr^+$ monocations do on the pyrrolidinium ring. This distinct behavior in the orbital level suggests the intrisic difference in oxidation mechanism between the dication and monocation regardless of the introduction of ether chain, although this is not experimentally validated in the present study because the anodic stability of the $PO_2F_2^-$ DILs is mainly determined by the anion as shown below.

The comparison of the theoretical electrochemical stabilities of the cations and anions

reveals that the cathodic limits of the ILs considered here are determined by the reduction of the cations due to the high cathodic stabilities of BF_4^- and $PO_2F_2^-$. However, this discussion is not validated in the present work because of the complicated reduction waves observed here (Figure 5). On the other hand, the lower anodic limits of the $PO_2F_2^-$ DILs ($[C_{1O2O1}\text{-}(C_1pyrr)_2][PO_2F_2]_2$ and $[C_{1O2O1}\text{-}(N_{221})_2][PO_2F_2]_2$) than the BF_4^- DIL ($[C_{1O2O1}\text{-}(C_1pyrr)_2][BF_4]_2$) (Figure 6) are endorsed by the lower anodic stability of $PO_2F_2^-$ than that of BF_4^-.

Conclusion

In conclusion, a series of dicationic salts with $PO_2F_2^-$ were synthesized in this study. Introduction of ether linker lowers their melting points (C_{1O2O1} linker vs. C_6 linker), leading to the three room-temperature DILs $[C_{1O2O1}\text{-}(C_1pyrr)_2][PO_2F_2]_2$, $[C_{1O2O1}\text{-}(N_{221})_2][PO_2F_2]_2$, and $[C_{1O2O1}\text{-}(C_1pyrr)_2][BF_4]_2$. When comparing the pyrrolidinium and tetraalkylammonium structures, the pyrrolidinium-based DILs exhibited lower viscosity and higher ionic conductivity. In addition, $[C_{1O2O1}\text{-}(C_1pyrr)_2][PO_2F_2]_2$ showed lower viscosity and higher conductivity than $[C_{1O2O1}\text{-}(C_1pyrr)_2][BF_4]_2$, which suggests that the decrease of the cation-anion interaction by the larger size of $PO_2F_2^-$ than BF_4^- overcomes the increased dipole moment of $PO_2F_2^-$. Both the $PO_2F_2^-$ and BF_4^- DILs have a higher anodic stability compared to the corresponding monocationic ILs, as suggested by the electrochemical stabilities based on DFT calculations. Such tolerance to oxidation is beneficial for their future application in high voltage batteries, and a valuable future direction would be to assess the performance of these DILs in energy storage devices.

Experimental Section

Apparatus and Materials. Volatile materials were handled with air-tight glass equipment

(SPC series, SIBATA Co.) and in a glass vacuum line. Nonvolatile materials were handled under a dry Ar atmosphere in a glovebox or a dry air atmosphere in an open dry chamber. The deuterated solvents (dimethyl sulfoxide (DMSO)-d_6 containing 0.05 vol% tetramethylsilane (TMS), Wako Chemicals, purity 99.9%; DMSO-d_6, Aldrich, purity 99.9%; $CDCl_3$ containing 0.05vol% TMS, Wako Chemicals, purity 99.8%) and ^{19}F NMR and ^{31}P NMR reference samples (hexafluorobenzene, Wako Chemicals, purity > 99.0% and tributyl phosphate, Wako Chemicals, purity > 98.0%) were used as purchased. The solvents and reagents, dichloromethane (Wako Chemicals, purity >99.5%), acetone (Wako Chemicals, purity 99.5%), and diethyl ether (Wako Chemicals, purity >99.5%), [K][PO_3] (Wako Chemicals, purity 99.5%), [K][PF_6] (purity 57.0~80.0wt%), [K][BF_4] (Wako Chemicals, purity >99.0%), [Li][TFSA] (Tokyo Chemical Industry Co., Ltd., purity >98.0%)), paraformaldehyde (Tokyo Chemical Industry Co., Ltd., purity >90.0%), calcium chloride (Wako Chemicals, purity >95.0%), ethylene glycol (Wako Chemicals, purity >99.5%), chlorotrimethylsilane (Tokyo Chemical Industry, purity >98.0%), *N*-methylpyrrolidine (Tokyo Chemical Industry Co., Ltd., purity >98.0%), *N*,*N*-diethylmethylamine (Tokyo Chemical Industry Co., Ltd., purity >98.0%), and *N*-methylimidazole (Tokyo Chemical Industry Co., Ltd., purity >99.0%) were used as purchased. [K][PO_2F_2] was prepared by the reaction of [K][PO_3] and [K][PF_6] at 320 ℃ according to a previous report.[26] The purity of the obtained sample was confirmed by X-ray powder diffraction.[51] All the obtained compounds were characterized by NMR and IR spectroscopy. The chloride ion contents of the DILs were below 0.1 wt% according to the results of X-ray fluorescence spectroscopy.

Synthesis of 1,2-bis(chloromethoxy)ethane. According to a previous report,[25] 1,2-bis(chloromethoxy)ethane was prepared as follows. Dichloromethane (100 cm^3) was added to

paraformaldehyde (10.02 g, 333.6 mmol) and calcium chloride at room temperature, and the mixture was agitated for 1 h. Then, ethylene glycol (7.564 g, 121.9 mmol) and chlorotrimethylsilane (46 cm^3) were added to the mixture. A colorless liquid and a white precipitate were obtained after agitation under an Ar atmosphere for 21h at room temperature. The white precipitation and volatiles were removed by filtration and evacuation with a rotary evaporator at 40 °C. Finally, 1,2-bis(chloromethoxy)ethane was obtained as a colorless liquid by purification through vacuum distillation at 100 °C (11.29 g, 71.5 mmol). ^{1}H NMR (399.8 MHz, $CDCl_3$, ppm): δ = 3.90 (s, 4H, C*H*$_2$OCH$_2$Cl), 5.53 (s, 4H, CH$_2$OC*H*$_2$Cl). IR (ATR, cm^{-1}): 571 (sh), 628 (vs), 846 (m), 908 (w), 934 (vw), 975 (sh), 1007 (sh), 1038 (s), 1103 (sh), 1112 (vs), 1250 (w), 1269 (w), 1320 (w), 1450 (vw), 1460 (vw), 2890 (vw), 2945 (vw).

Synthesis of [C_{1O2O1}-(C_1pyrr)$_2$][Cl]$_2$. Into a round-bottom flask containing 100 cm^3 of dichloromethane, *N*-methylpyrrolidine (12.80 g, 150.3 mmol), and 1,2-bis(chloromethoxy)ethane (11.29 g, 71.46 mmol) were added. The resulting solution was stirred for 16 h at room temperature. After the removal of volatiles under vacuum, the resulting yellow solid was washed with 100 cm^3 of diethyl ether three times to remove unreactive reagents. The solvent was roughly removed under vacuum with a rotary evaporator at 40 °C. A yellow solid of [C_{1O2O1}-(C_1pyrr)$_2$][Cl]$_2$ was obtained (22.44 g, 68.38 mmol) by further drying under vacuum at room temperature overnight and then at 70 °C for 10 h. ^{1}H NMR (399.8 MHz, DMSO-d_6, ppm) δ = 2.08-2.13 (m, 8H, NCH$_2$C*H*$_2$C*H*$_2$), 3.09 (s, 6H, NC*H*$_3$), 3.43-3.58 (m, 8H, NC*H*$_2$C), 4.04 (s, 4H, OC*H*$_2$C*H*$_2$O), 4.94 (s, 4H, NC*H*$_2$O). IR (ATR, cm^{-1}): 412 (vw), 421 (vw), 462 (w), 528 (w), 563 (vw), 614 (w), 645 (w), 730 (vw), 829 (m), 847 (vw), 905 (sh), 913 (s), 956 (sh), 998 (vw), 1024 (w), 1047 (vw), 1115 (s), 1144 (vs), 1185 (m), 1245 (vw), 1255 (vw), 1270 (vw), 1305 (sh), 1319 (vw), 1352 (vw), 1383 (vw), 1406 (vw), 1422 (vw), 1460 (m), 1469 (sh), 2970 (w), 2968 (m), 2995 (sh).

Synthesis of $[C_{1O2O1}\text{-}(C_1pyrr)_2][PO_2F_2]_2$. A slightly excess amount of $[K][PO_2F_2]$ (11.79 g, 84.26 mmol) was added to $[C_{1O2O1}\text{-}(C_1pyrr)_2][Cl]_2$ (13.12 g, 40.00 mmol) in a round-bottom flask containing 80 cm^3 of acetone as a solvent. The mixture was stirred for two days, and the resulting white precipitate of KCl was removed by filtration. The solvent was removed under vacuum at room temperature and then later at 70 ℃ to yield $[C_{1O2O1}\text{-}(C_1pyrr)_2][PO_2F_2]_2$ as a colorless liquid (15.59 g, 33.88 mmol). ^{1}H NMR (399.8 MHz, DMSO-d_6, ppm): δ = 2.06-2.13 (m, 8H, $NCH_2CH_2CH_2$), 3.01 (s, 6H, NCH_3), 3.37-3.50 (m, 8H, NCH_2CH_2), 3.99 (s, 4H, OCH_2CH_2O), 4.74 (s, 4H, NCH_2O) ^{19}F NMR (564.7 MHz, DMSO-d_6, ppm): δ = −80.7 (d, J = 951.5 Hz, $PO_2F_2^-$). ^{31}P NMR (161.8 MHz, DMSO-d_6, ppm): δ = −15.9 (t, J = 951.2 Hz, $PO_2F_2^-$). IR (ATR, cm^{-1}): 490 (vs), 532 (vw), 647 (vw), 804 (vs), 922 (w), 989 (vw), 1022 (w), 1128 (vs), 1183 (sh), 1297 (vs), 1313 (vs), 1458 (m), 2892 (sh), 2968 (w), 3026 (vw). Water content: 291 ppm.

Synthesis of $[C_{1O2O1}\text{-}(C_1pyrr)_2][BF_4]_2$. The same procedure as that for $[C_{1O2O1}\text{-}(C_1pyrr)_2][PO_2F_2]_2$ was used. Reaction of $[C_{1O2O1}\text{-}(C_1pyrr)_2][Cl]_2$ (7.868 g, 23.98 mmol) and $[K][BF_4]$ (6.188 g, 49.15 mmol) in 100 cm^3 of acetone gave $[C_{1O2O1}\text{-}(C_1pyrr)_2][BF_4]_2$ as yellow liquid (9.273 g, 21.45 mmol). ^{1}H NMR (600.2 MHz, DMSO-d_6, ppm): δ = 2.06-2.14 (m, 8H, $NCH_2CH_2CH_2$), 3.02 (s, 6H, NCH_3), 3.38-3.48(m, 8H, NCH_2C), 4.00 (s, 4H, OCH_2CH_2O), 4.74 (s, 4H, NCH_2O). ^{19}F NMR (376 MHz, DMSO-d_6, ppm): δ = −150.5 (s, $^{10}BF_4^-$), −150.6 (s, $^{11}BF_4^-$). IR (ATR, cm^{-1}): 520 (m), 555 (m), 640 (vw), 740 (sh), 765 (sh), 824 (s), 926 (w), 1022 (vs), 1024 (sh), 1138 (sh), 1256 (vw), 1285 (vw), 1299 (sh), 1367 (vw), 1466 (m), 2896 (sh), 2955 (w), 3047 (vw). Water content: 521 ppm.

Synthesis of $[C_{1O2O1}\text{-}(N_{221})_2][Cl]_2$. The same procedure as that for $[C_{1O2O1}\text{-}(C_1pyrr)_2][Cl]_2$ was used. Reaction of *N*,*N*-diethylmethylamine (11.73 g, 134.6 mmol) and 1,2-bis(chloromethoxy)ethane (10.16 g, 64.31 mmol) in 100 cm^3 of dichloromethane gave $[C_{1O2O1}$-

$(N_{221})_2][Cl]_2$ as a white solid (21.24 g, 64.72 mmol). ^{1}H NMR (600.2 MHz, DMSO-d_6, ppm): δ = 1.22 (t, J = 7.2 Hz, 12H, NCH_2CH_3), 2.95 (s, 6H, NCH_3), 3.29-3.38 (m, 8H, NCH_2CH_2), 4.00 (s, 4H, OCH_2CH_2O), 4.85 (s, 4H, NCH_2O). IR (cm^{-1}): 416 (vw), 439 (vw), 481 (vw), 596 (w), 706 (w), 798 (s), 816 (sh), 851 (m), 869 (w), 889 (w), 960 (w), 968 (w), 1014 (s), 1085 (sh), 1105 (s), 1116 (s), 1146 (vs), 1199 (w), 1216 (sh), 1269 (vw), 1299 (sh), 1316 (w), 1354 (vw), 1383 (sh), 1403 (m), 1428 (sh), 1452 (s), 1483 (sh), 2886 (vw), 2937 (sh), 2974 (m), 3000 (sh).

Synthesis of $[C_{1O2O1}\text{-}(N_{221})_2][PO_2F_2]_2$. The same procedure as that for $[C_{1O2O1}\text{-}(C_1pyrr)_2][PO_2F_2]_2$ was used. Reaction of $[C_{1O2O1}\text{-}(N_{221})_2][Cl]_2$ (7.254 g, 21.84 mmol) and $[K][PO_2F_2]$ (6.449 g, 46.09 mmol) in 100 cm^3 of acetone gave $[C_{1O2O1}\text{-}(C_1pyrr)_2][PO_2F_2]_2$ as colorless liquid (9.001 g, 19.39 mmol). ^{1}H NMR (600.2 MHz, DMSO-d_6, ppm): δ = 1.12-1.24 (t, J = 7.5 Hz, 12H, NCH_2CH_3), 2.90 (s, 6H, NCH_3), 3.25-3.32 (m, 8H, NCH_2CH_2)), 3.97 (s, 4H, OCH_2CH_2O), 4.70 (s, 4H, NCH_2O). ^{19}F NMR (564.7 MHz, DMSO-d_6, ppm): δ = −80.6 (d, J =951.5 Hz, $PO_2F_2^-$). ^{31}P NMR (243.0 MHz, DMSO-d_6, ppm): δ = −16.0 (t, J = 952.2 Hz, $PO_2F_2^-$). IR (ATR, cm^{-1}): 494 (vs), 712 (sh), 800 (vs), 889 (vw), 965 (vw), 1012 (w), 1026 (sh), 1105 (sh), 1132 (vs), 1193 (w), 1212 (sh), 1299 (vs), 1316 (vs), 1367 (vw), 1399 (vw), 1462 (m), 1481 (sh), 2894 (vw), 2951 (sh), 2990 (w), 3015 (sh). Water content: 355 ppm.

Synthesis of $[C_6\text{-}(C_1pyrr)_2][Cl]_2$. Into a round-bottom flask containing *N*-methylpyrrolidine (10.64 g, 125.0 mmol) and 1,6-dichlorohexane (7.814 g, 50.39 mmol) were added. After refluxing for 24 h at 70 ℃, the product was purified in the same procedure as that for $[C_{1O2O1}\text{-}(C_1pyrr)_2][Cl]_2$. The product of $[C_6\text{-}(C_1pyrr)_2][Cl]_2$ was obtained as a white solid (5.769 g, 17.79 mmol). ^{1}H NMR (399.8 MHz, DMSO-d_6, ppm): δ = 1.32-1.36 (br, 4H, $NCH_2CH_2CH_2$(linker)), 1.71-1.72 (br, 4H, NCH_2CH_2(linker)), 2.08-2.12 (br, 8H, $NCH_2CH_2CH_2$(ring)), 2.99 (s, 6H, NCH_3), 3.29-3.32 (m, 4H, NCH_2(linker)), 3.41-3.43 (m, 8H,

NC*H*$_2$CH$_2$(ring)). IR (ATR, cm^{-1}) 412 (w), 449 (w), 581 (vw), 612 (w), 657 (w), 738 (sh), 773 (vs), 832 (m), 891 (w), 906 (s), 916 (s), 936 (w), 963 (vw), 979 (vw), 1010 (m), 1046 (w), 1087 (vw), 1116 (vw), 1169 (vw), 1242 (vw), 1260 (vw), 1303 (w), 1342 (vw), 1371 (m), 1383 (vw), 1429 (vw), 1462 (vs), 1477 (sh), 2835 (vw), 2884 (vw), 2951 (sh), 2982 (vs), 3000 (sh).

Synthesis of [C$_6$-(C$_1$pyrr)$_2$][PO$_2$F$_2$]$_2$. The same procedure as that for [C$_{1O2O1}$-(C$_1$pyrr)$_2$][PO$_2$F$_2$]$_2$ was used. Reaction of [C$_6$-(C$_1$pyrr)$_2$][Cl]$_2$ (4.894 g, 15.10 mmol) and [K][PO$_2$F$_2$] (4.314 g, 30.83 mmol) in 100 cm^3 of acetone gave [C$_1$O$_2$O$_1$-(C$_1$pyrr)$_2$][PO$_2$F$_2$]$_2$ as white solid (3.260 g, 7.146 mmol).^{1}H NMR (600.2 MHz, DMSO-d_6, ppm): δ = 1.29-1.36 (m, 4H, NCH$_2$CH$_2$C*H*$_2$(linker)), 1.64-1.76 (br, 4H, NCH$_2$C*H*$_2$(linker)), 2.03-2.14 (br, 8H, NCH$_2$C*H*$_2$C*H*$_2$(ring)), 2.98 (s, 6H, NC*H*$_3$), 3.27-3.35 (m, 4H, NC*H*$_2$(linker)), 3.41-3.49 (m, 8H N−C*H*$_2$−CH$_2$(ring)). ^{19}F NMR (376.2 MHz, DMSO-d_6, ppm): δ = −80.6 (d, J = 951.0 Hz, PO$_2$*F*$_2^-$). ^{31}P NMR (243.0 MHz, DMSO-d_6, ppm): δ = −15.92 (t, J = 953.8Hz, *P*O$_2$F$_2^-$). IR (ATR, cm^{-1}): 494 (vs), 571 (m), 645 (w), 734 (m), 804 (vs), 932 (w), 963 (vw), 1006 (vw), 1018 (sh), 1048 (vw), 1108 (sh), 1134 (vs), 1181 (m), 1216 (vw), 1301 (sh), 1317 (vs), 1362 (vw), 1383 (w), 1434 (sh), 1469 (w), 2866 (vw), 2941 (w), 3027 (sh).

Synthesis of [C$_{1O2O1}$-(C$_1$im)$_2$][Cl]$_2$. The same procedure as that for [C$_{1O2O1}$-(C$_1$pyrr)$_2$][Cl]$_2$ was used. Reaction of *N*-methylimidazole (5.301 g, 64.57 mmol) and 1,2-bis(chloromethoxy)ethane (4.820 g, 30.51 mmol) in 50 cm^3 of dichloromethane gave [C$_{1O2O1}$-(N$_{221}$)$_2$][Cl]$_2$ as white solid (8.362 g, 64.72 mmol). ^{1}H NMR (600.2 MHz, DMSO-d_6, ppm): δ = 3.69 (s, 4H, OC*H*$_2$C*H*$_2$O), 3.92 (s, 6H, NC*H*$_3$), 5.64 (s, 4H, NC*H*$_2$O), 7.81 (t, J = 1.8Hz, 2H, NC*H*CHNCH$_3$), 7.92 (t, J = 1.8Hz, 2H, NCHC*H*NCH$_3$), 9.58 (s, 2H, NC*H*N). IR (ATR, cm^{-1}): 408 (vw), 426 (w), 432 (vw), 465 (vw), 528 (vw), 612 (sh), 618 (s), 646 (vw), 660 (w), 747 (s), 765 (sh), 838 (m), 893 (m), 902 (sh), 924 (vw), 953 (vw), 1008 (sh), 1024 (m), 1093 (vs), 1120 (vs), 1154 (s), 1185 (sh), 1244 (vw), 1277 (vw), 1309 (vw), 1381 (vw), 1403 (vw), 1440 (vw),

1464 (vw), 1479 (sh), 1560 (sh), 1570 (w), 2974 (w), 2996 (sh), 3076 (vw), 3125 (vw), 3161 (vw).

Synthesis of $[C_{1O2O1}\text{-}(C_1im)_2][PO_2F_2]_2$. The same procedure as that for $[C_{1O2O1}\text{-}(C_1pyrr)_2][PO_2F_2]_2$ was used. Reaction of $[C_{1O2O1}\text{-}(C_1im)_2][Cl]_2$ (6.966 g, 21.63 mmol) and $[K][PO_2F_2]$ (6.249 g, 44.66 mmol) in 100cm^3 of acetone gave $[C_{1O2O1}\text{-}(C_1pyrr)_2][PO_2F_2]_2$ as white solid (9.162 g, 20.18 mmol). ^{1}H NMR (600.2 MHz, DMSO-d_6, ppm): δ = 3.76 (s, 4H, OCH_2CH_2O), 3.89 (s, 6H, NCH_3), 5.57 (s, 4H, NCH_2O), 7.78 (t, J = 1.50 Hz, 2H, NCHCHNCH$_3$), 7.84 (t, J = 1.80 Hz, 2H, NCHCHNCH$_3$), 9.29 (s, 2H, NCHN). ^{19}F NMR (376.2 MHz, DMSO-d_6, ppm): δ = −80.6 (d, $^1J(^{31}P–^{19}F)$ = 952.2 Hz, $PO_2F_2^-$). ^{31}P NMR (161.8 MHz, DMSO-d_6, ppm): δ = −16.0 (t, $^1J(^{31}P–^{19}F)$ = 951.8 Hz, $PO_2F_2^-$). IR (ATR, cm^{-1}): 492 (vs), 612 (sh), 624 (m) 673 (w), 738 (m), 802 (vs), 1026 (sh), 1101 (sh), 1132 (vs), 1161 (sh), 1297 (vs), 1299 (vs), 1367 (vw), 1399(sh), 1422(vw), 1458 (vw), 1560 (w), 1579 (w), 2880 (vw), 2961 (vw), 3031 (sh), 3087 (w), 3149 (vw).

Spectroscopic and Thermal Analysis.

Infrared spectra were recorded by a Fourier transform IR spectrometer (ALPHA II, Bruker Optics Laboratories, Inc.) equipped with an attenuated total reflection (ATR) module under the dry air atmosphere. Nuclear magnetic resonance spectra of ^{1}H, ^{13}C and ^{19}F (600 or 400 MHz) were recorded (JEOL JSM-ECA600NMR spectrometer or JEOL JSM-ECA400NMR spectrometer) at room temperature. Deuterated DMSO was used as a solvent for all the measurements. The chemical shift of the obtained spectra was shown with reference to TMS, CCl_3F, and 85% H_3PO_4 for ^{1}H, ^{19}F, and ^{31}P NMR. Thermal behavior was measure by differential scanning calorimetry (DSC8230, Rigaku Thermo Plus EVO II Series) under a dry Ar gas flow or in the air at a scan rate of 5 ℃ min^{-1}. The samples for DSC measurements were loaded into an aluminum airtight cell under dry Ar.

Measurement of Physical and Electrochemical Properties.

Densities were measured using an oscillating U-tube density meter (DMA 4500 M, Anton Paar GmbH). Viscosities were measured with an electromagnetically spinning viscometer EMS-100 (Kyoto Electronics Manufacturing Co., Ltd.). Samples were sealed in glass tubes with a spherical Al probe in the glove box. Ionic conductivities were measured using the AC impedance technique with the aid of an impedance analyzer (3532-80, Hioki E.E. Corp.). The samples for the ionic conductivity measurements were sealed in an atmosphere of dry Ar into an airtight T-shaped cell equipped with stainless steel disk electrodes. The cell was placed in a thermostatic chamber (SU-241, ESPEC) and held at each measurement temperature for 30 min prior to measurements. The water contents were measured using the Karl Fischer titration method (899 Coulometer, Metrohm). The chloride ion contents analyzed by X-ray fluorescence spectroscopy (EDXL 300, Rigaku Corp.) under a He atmosphere. Cyclic voltammetry was performed on a three-electrode beaker cell using a glass-like carbon working electrode and graphite counter electrode. The reference electrode was made of silver wire immersed in $[C_2C_1im][FSA]$ containing 0.05 mol dm^{-3} of $[Ag][SO_3CF_3]$ that was separated from the test electrolyte with porous glass.

X-Ray Diffraction Analyses.

The XRD pattern was recorded in the Bragg−Brentano geometry using a Rigaku MiniFlex diffractometer with Ni-filtered CuKα radiation (30 kV and 10 mA) and a D/tex Ultra250 Si-strip high-speed detector. Data were collected over a 2θ range of 10 to 80 deg with a step size of 0.01 and scan rate of 1 deg min^{-1}.

Calculations.

The energy-minimized structures were obtained by the DFT calculation at the PBE1PBE level of theory using the aug-cc-pVDZ basis set.[52-55] Closed-shell restricted wavefunctions were

used to calculate the cations and anions, while unrestricted open-shell wavefunctions were used for the ions that have singly occupied orbitals. Energy minimum of each optimized structure was confirmed by frequency analysis, which was further used for thermochemical corrections to obtain Gibbs energies. The PCM calculations were performed using a dielectric constant of 15 which is typical of ILs.[56-58] Quantum mechanical calculations were carried out using the program Gaussian 16. [59]

Conflicts of interest

The authors declare no competing financial interest.

Acknowledgements

One of the authors, K. K, thanks to JST SPRING Grant Number JPMJSP2110 for th efinancial support. This work was supported by funding from Sumitomo Chemical Co., Ltd.

References

(1)Z. G. Lei, B. H. Chen, Y. M. Koo and D. R. MacFarlane, *Chem. Rev.*, 2017, **10**, 6633-6635.

(2)G. Kaur, H. Kumar and M. Singla, *J. Mol. Liq.*, 2022, 118556.

(3)H. Xue, R. Verma and J. M. Shreeve, *J. Fluorine Chem.*, 2006, **2**, 159-176.

(4)R. Hayes, G. G. Warr and R. Atkin, *Chem. Rev.*, 2015, **13**, 6357-6426.

(5)M. Watanabe, M. L. Thomas, S. G. Zhang, K. Ueno, T. Yasuda and K. Dokko, *Chem. Rev.*, 2017, **10**, 7190-7239.

(6)Y. Y. Zheng, D. Wang, S. Kaushik, S. N. Zhang, T. Wada, J. Hwang, K. Matsumoto and R. Hagiwara, *Energychem*, 2022, **3**, 100075.

(7)M. Galinski, A. Lewandowski and I. Stepniak, *Electrochim. Acta*, 2006, **26**, 5567-5580.

(8)M. Armand, F. Endres, D. R. MacFarlane, H. Ohno and B. Scrosati, *Nat. Mater.*, 2009, **8**, 621-629.

(9)A. Lewandowski and A. Swiderska-Mocek, *J. Power Sources*, 2009, **2**, 601-609.

(10)X. Y. Ma, J. T. Yu, Q. Y. Dong, X. Y. Zou, L. Zheng, Y. Hu, Y. B. Shen, L. W. Chen and F. Yan, *ACS Appl. Mater. Interfaces*, 2022, **36**, 41103-41113.

(11)A. Celeste, L. Silvestri, M. Agostini, M. Sadd, S. Palumbo, J. C. Panda, A. Matic, V. Pellegrini and S. Brutti, *Batter. Supercaps*, 2020, **10**, 1059-1068.

(12)P. Barthen, W. Frank and N. Ignatiev, *Ionics*, 2015, **1**, 149-159.

(13)A. n. Masri, M. I. A. Mutalib and J.-M. Lévêque, *Ind. Eng. Manage.*, 2016, **4**, 197.

(14)T. Payagala, J. Huang, Z. S. Breitbach, P. S. Sharma and D. W. Armstrong, *Chem. Mater.*, 2007, **24**, 5848-5850.

(15)H. Shirota, T. Mandai, H. Fukazawa and T. Kato, *J. Chem. Eng. Data*, 2011, **5**, 2453-2459.

(16)M. G. Montalbán, G. Víllora and P. Licence, *Ecotoxicol. Environ. Saf.*, 2018, 129-135.

(17)T. C. Nirmale, N. D. Khupse, R. S. Kalubarme, M. V. Kulkarni, A. J. Varma and B. B. Kale, *ACS Sustain. Chem. Eng.*, 2022, **26**, 8297-8304.

(18)M. Talebi, R. A. Patil and D. W. Armstrong, *J. Mol. Liq.*, 2018, 247-255.

(19)F. Pandolfi, M. Bortolami, M. Feroci, A. Fornari, V. Scarano and D. Rocco, *Materials*, 2022, **3**, 866.

(20)C. S. Perez-Martinez and S. Perkin, *Langmuir*, 2019, **48**, 15444-15450.

(21)I. M. Gindri, D. A. Siddiqui, P. Bhardwaj, L. C. Rodriguez, K. L. Palmer, C. P. Frizzo, M. A. P. Martins and D. C. Rodrigues, *RSC Adv.*, 2014, **107**, 62594-62602.

(22)J. L. Anderson, R. Ding, A. Ellern and D. W. Armstrong, *J. Am. Chem. Soc.*, 2004, **2**, 593-604.

(23)R. A. Patil, M. Talebi, C. D. Xu, S. S. Bhawal and D. W. Armstrong, *Chem. Mater.*, 2016, **12**, 4315-4323.

(24)A. R. C. Morais, L. M. Alaras, D. L. Baek, R. V. Fox, M. B. Shiflett and A. M. Scurto, *J. Chem. Eng. Data*, 2019, **11**, 4658-4667.

(25)T. Nokami, T. Yamashita, T. Komura, N. Handa, M. Shimizu, K. Yamaguchi, Y. Domi, H. Usui, H. Sakaguchi and T. Itoh, *Faraday Discuss.*, 2018, 523-534.

(26)K. Matsumoto and R. Hagiwara, *Inorg. Chem.*, 2009, **15**, 7350-7358.

(27)D. S. Hall, T. Hynes, C. P. Aiken and J. R. Dahn, *J. Electrochem. Soc.*, 2020, **10**, 100538.

(28)A. P. Wang, L. Wang, H. M. Liang, Y. Z. Song, Y. F. He, Y. Z. Wu, D. S. Ren, B. Zhang and X. M. He, *Adv. Funct. Mater.*, 2023, **8**, 2211958.

(29)P. C. Shi, L. C. Zhang, H. F. Xiang, X. Liang, Y. Sun and W. Xu, *ACS Appl. Mater. Interfaces*, 2018, **26**, 22201-22209.

(30)H. Yang, J. Hwang, Y. Tonouchi, K. Matsumoto and R. Hagiwara, *J. Mater. Chem. A*, 2021, **6**, 3637-3647.

(31)H. Yang, C. Y. Chen, J. Hwang, K. Kubota, K. Matsumoto and R. Hagiwara, *ACS Appl. Mater. Interfaces*, 2020, **32**, 36168-36176.

(32)G. Yang, J. Shi, C. Shen, S. Wang, L. Xia, H. Hu, H. Luo, Y. Xia and Z. Liu, *RSC Adv.*, 2017, **42**, 26052.

(33)V. G. Krasovskii, G. I. Kapustin, L. M. Glukhov, E. A. Chernikova and L. M. Kustov, *Russ. J. Phys. Chem. A*, 2023, **9**, 1914-1922.

(34)Z. Katcharava, F. Navazandeh-Tirkalaee, T. E. Orlamünde, K. Busse, S. J. Kinkelin, M. Beiner, A. Marinow and W. H. Binder, *Chem. Eur. J.*, 2024, **54**, e202402004.

(35)J. F. Vélez, M. B. Vázquez-Santos, J. M. Amarilla, B. Herradón, E. Mann, C. del Río and E. Morales, *J. Power Sources*, 2019, 227098.

(36)K. Matsumoto, T. Okawa and R. Hagiwara, *Chem. Lett.*, 2012, **4**, 394-396.

(37)H. Vogel, *Phys. Z.*, 1921, 645-646.

(38)G. Tammann and W. Hesse, *Z. Anorg. Allg. Chem.*, 1926, **4**, 19261560121.

(39)G. S. Fulcher, *J. Am. Ceram. Soc.*, 1925, **6**, 339-355.

(40)W. Xu, E. I. Cooper and C. A. Angell, *J. Phys. Chem. B*, 2003, **25**, 6170-6178.

(41)H. Tokuda, K. Hayamizu, K. Ishii, M. Abu Bin Hasan Susan and M. Watanabe, *J. Phys. Chem. B*, 2004, **42**, 16593-16600.

(42)A. Noda, K. Hayamizu and M. Watanabe, *J. Phys. Chem. B*, 2001, **20**, 4603–4610.

(43)H. S. a. K. T. H. Matsumoto, *ECS Trans.*, 2009, **35**, 59-66.

(44)J. Reiter, E. Paillard, L. Grande, M. Winter and S. Passerini, *Electrochim. Acta*, 2013, 101-107.

(45)K. Matsumoto, R. Hagiwara, R. Yoshida, Y. Ito, Z. Mazej, P. Benkic, B. Zemva, O. Tamada, H. Yoshino and S. Matsubara, *Dalton trans.*, 2004, **1**, 144-149.

(46)P. Walden, H. Ulich and G. Busch, *Z. Phys. Chem.*, 1926, **5/6**, 429-434.

(47)P. Walden and E. J. Birr, *Z. Phys. Chem., Abt. A*, 1931, **1/2**, 1-51.

(48)K. Matsumoto and R. Hagiwara, *J. Electrochem. Soc.*, 2010, **5**, A578-A581.

(49)V. Borgel, E. Markevich, D. Aurbach, G. Semrau and M. Schmidt, *J. Power Sources*, 2009, **1**, 331-336.

(50)S. P. Ong, O. Andreussi, Y. B. Wu, N. Marzari and G. Ceder, *Chem. Mater.*, 2011, **11**, 2979-2986.

(51)U. Schülke and R. Kayser, *Z. Anorg. Allg. Chem.*, 1991, 221-226.

(52)C. Adamo and V. Barone, *J. Chem. Phys.*, 1999, **13**, 6158-6170.

(53)E. R. Davidson, *Chem. Phys. Lett.*, 1996, **3-4**, 514-518.

(54)T. H. Dunning, *J. Chem. Phys.*, 1989, **2**, 1007-1023.

(55)D. E. Woon and T. H. Dunning, *J. Chem. Phys.*, 1993, **2**, 1358-1371.

(56)E. Cances, B. Mennucci and J. Tomasi, *J. Chem. Phys.*, 1997, **8**, 3032-3041.

(57)C. Wakai, A. Oleinikova, M. Ott and H. Weingärtner, *J. Phys. Chem. B*, 2005, **36**, 17028-17030.

(58)H. Weingärtner, *J. Mol. Liq.*, 2014, 185-190.

(59)M. J. Frisch, G. W. Trucks, H. B. Schlegel, G. E. Scuseria, M. A. Robb, J. R. Cheeseman, G. Scalmani, V. Barone, G. A. Petersson, H. Nakatsuji, X. Li, M. Caricato, A. V. Marenich, J. Bloino, B. G. Janesko, R. Gomperts, B. Mennucci, H. P. Hratchian,

J. V. Ortiz, A. F. Izmaylov, J. L. Sonnenberg, D. Williams-Young, F. Ding, F. Lipparini, F. Egidi, J. Goings, B. Peng, A. Petrone, T. Henderson, D. Ranasinghe, V. G. Zakrzewski, J. Gao, N. Rega, G. Zheng, W. Liang, M. Hada, M. Ehara, K. Toyota, R. Fukuda, J. Hasegawa, M. Ishida, T. Nakajima, Y. Honda, O. Kitao, H. Nakai, T. Vreven, K. Throssell, J. A. Montgomery, Jr., J. E. Peralta, F. Ogliaro, M. J. Bearpark, J. J. Heyd, E. N. Brothers, K. N. Kudin, V. N. Staroverov, T. A. Keith, R. Kobayashi, J. Normand, K. Raghavachari, A. P. Rendell, J. C. Burant, S. S. Iyengar, J. Tomasi, M. Cossi, J. M. Millam, M. Klene, C. Adamo, R. Cammi, J. W. Ochterski, R. L. Martin, K. Morokuma, O. Farkas, J. B. Foresman and D. J. Fox. *G aussian 16, Revision C.01*; Gaussian, Inc., 2016.

Table 1 Physical and electrochemical properties of DILs based on $PO_2F_2^-$ and BF_4^-.[a]

	$[C_{1O2O1}\text{-}(C_1pyrr)_2][PO_2F_2]_2$	$[C_{1O2O1}\text{-}(N_{221})_2][PO_2F_2]_2$	$[C_{1O2O1}\text{-}(C_1pyrr)_2][BF_4]_2$
T_g (K)	200	205	224
ρ (g cm^{-3})	1.349	1.277	1.305
η (mPa s)	2000	3700	11900
σ (mS cm^{-1})	0.42	0.22	0.13
E_c (V)	−3.01	−2.37	−2.11
E_a (V)	1.90	1.90	2.80
EW (V)	4.91	4.27	4.91

[a] T_g: glass transition temperature, physical properties, ρ: density, η: viscosity, σ: ionic conductivity, E_c: cathode limit, E_a: anode limit, and EW: electrochemical widow (threshold: 0.1mA cm^{-2}). These parameters were measured at 298 K.

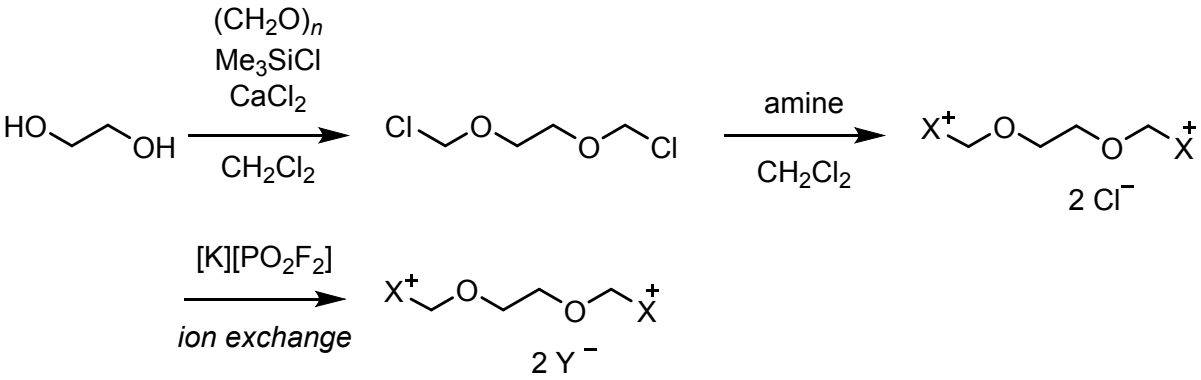

Scheme 1 The synthetic route of dicationic salts with ether linker ($[C_{1O2O1}\text{-}(C_1pyrr)_2][PO_2F_2]_2$, $[C_{1O2O1}\text{-}(N_{221})_2][PO_2F_2]_2$, $[C_{1O2O1}\text{-}(C_1im)_2][PO_2F_2]_2$, and $[C_{1O2O1}\text{-}(C_1pyrr)_2][BF_4]_2$). The X^+ and Y^- are an alkylammonium moiety and an anion, respectively.

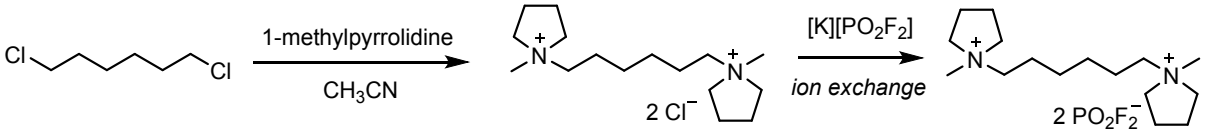

Scheme 2 The synthetic route of the $[C_6\text{-}(C_1pyrr)_2][PO_2F_2]_2$ DIL.

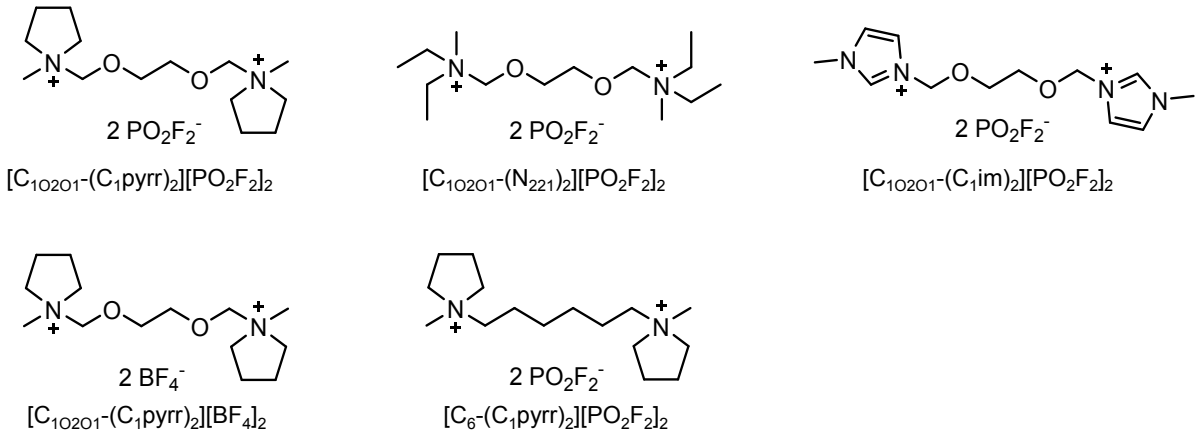

Figure 1 Structures and abbreviations of DILs in this study.

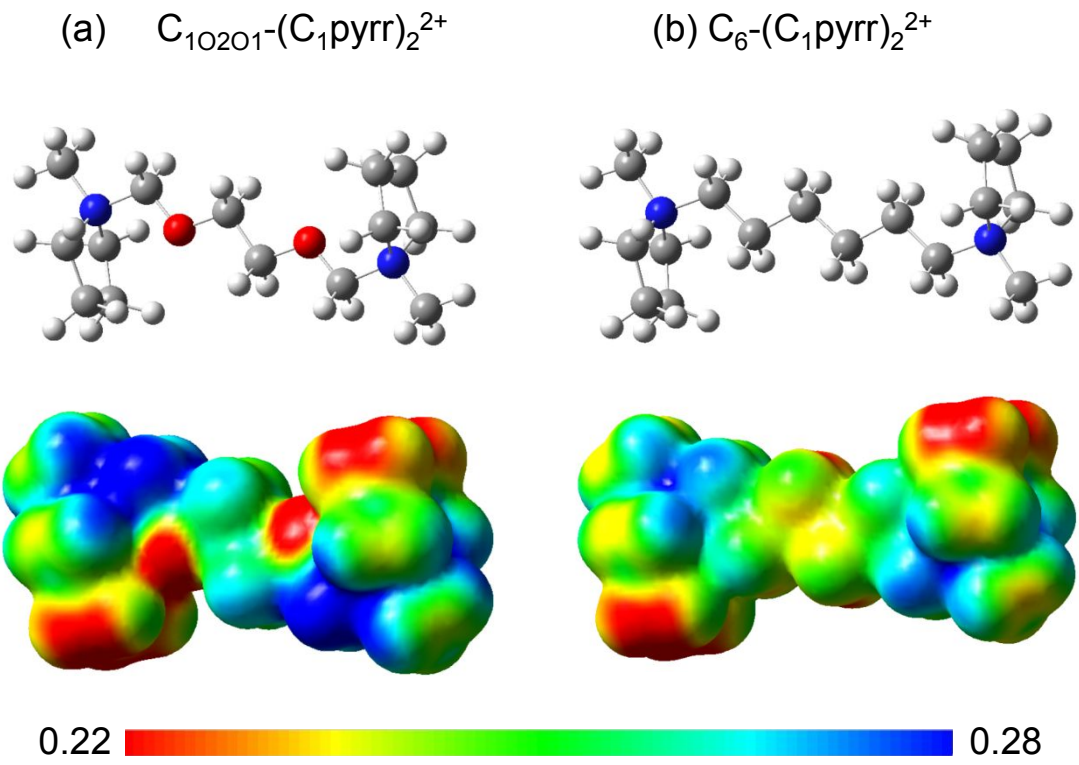

Figure 2 Optimized structures and electrostatic potential maps at the 0.005 e bohr^{-3} isosurfaces of (a) C_{1O2O1}-$(C_1pyrr)_2^{2+}$ and C_6-$(C_1pyrr)_2^{2+}$.

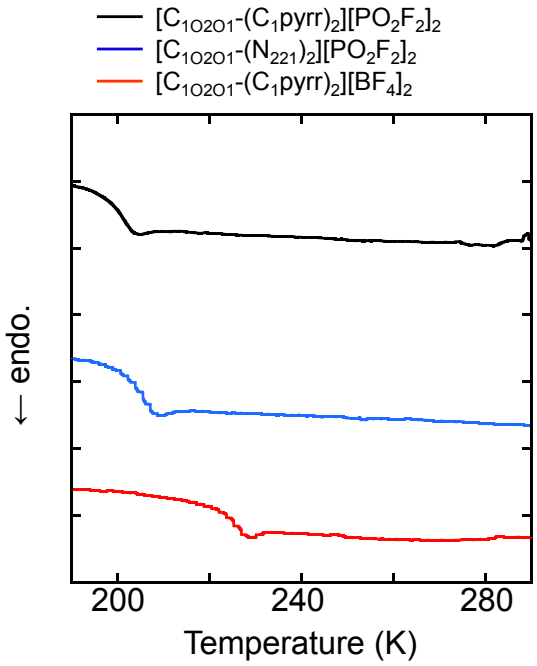

Figure 3 DSC curves of $[C_{1O2O1}\text{-}(C_1pyrr)_2][PO_2F_2]_2$, $[C_{1O2O1}\text{-}(N_{221})_2][PO_2F_2]_2$, and $[C_{1O2O1}\text{-}(C_1pyrr)_2][BF_4]_2$ under Ar atmosphere. Scan rate: 5 K min^{-1}.

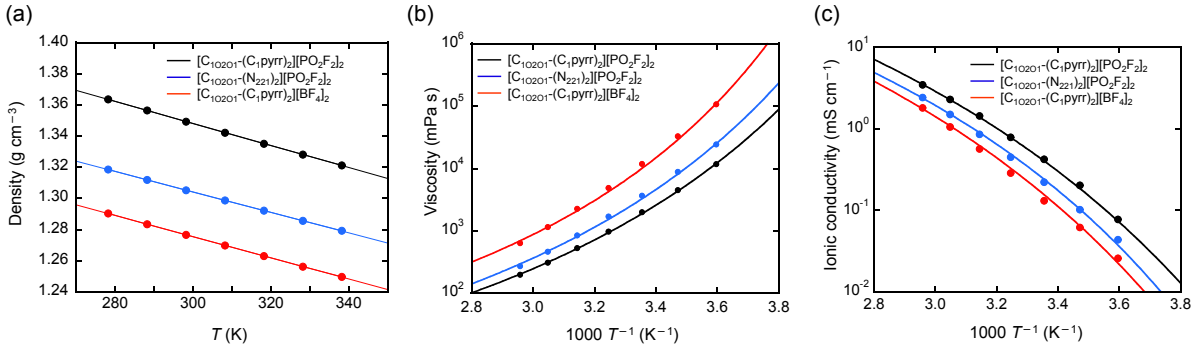

Figure 4 Temperature dependence of (a) densities, (b) viscosities, and (c) ionic conductivities for $[C_{1O2O1}\text{-}(C_1pyrr)_2][PO_2F_2]_2$, $[C_{1O2O1}\text{-}(N_{221})_2][PO_2F_2]_2$, and $[C_{1O2O1}\text{-}(C_1pyrr)_2][BF_4]_2$ (see Tables S1, S2, and S3 for the data of density, viscosity, and ionic conductivity).

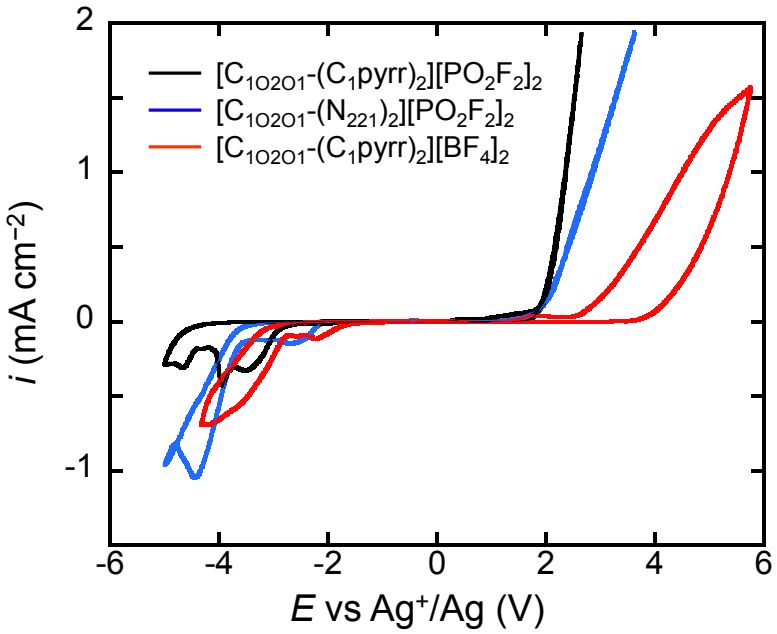

Figure 5 Cyclic voltammograms of a glass-like carbon electrode in $[C_{1O2O1}\text{-}(C_1pyrr)_2][PO_2F_2]_2$, $[C_{1O2O1}\text{-}(N_{221})_2][PO_2F_2]_2$, and $[C_{1O2O1}\text{-}(C_1pyrr)_2][BF_4]_2$. Scan rate: 5 mV s^{-1}.

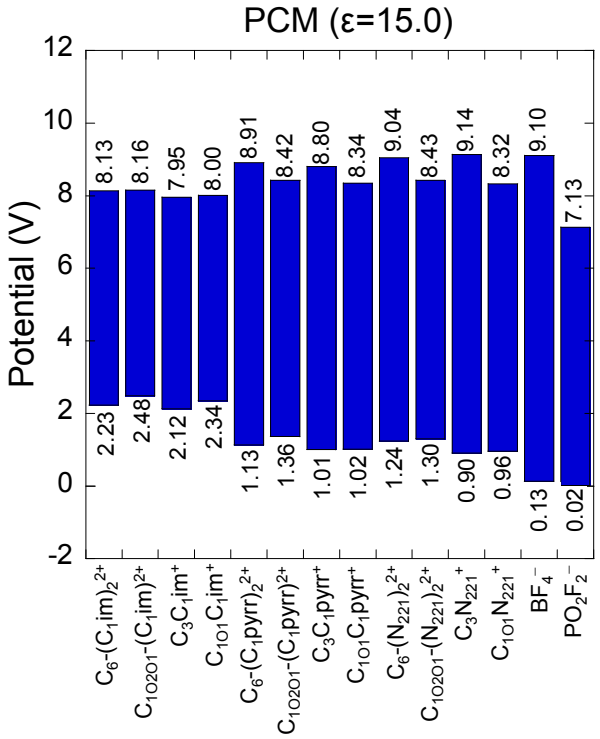

Figure 6 Electrochemical stabilities of the dications, monocations, and anions in this study calculated at the PBE1PBE/aug-cc-pVDZ level using the PCM model with a dielectric constant of 15. See Figure S1 for the structures of the chemical speices and Figure S4 for the electrochemical stabilities under vacuum.

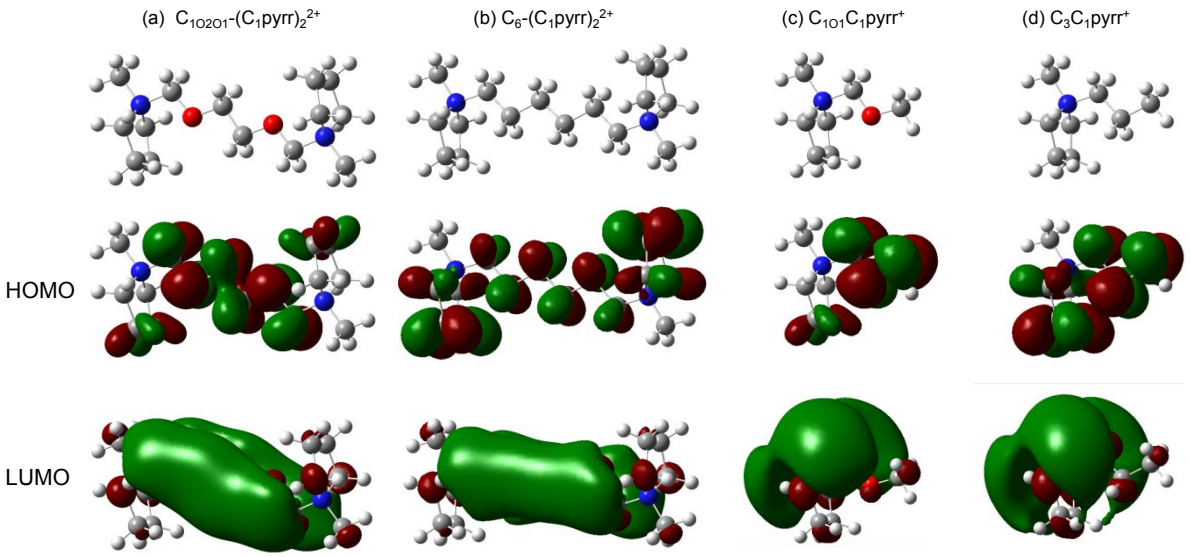

Figure 7 The HOMO and LUMO diagrams of (a) C_{1O2O1}-$(C_1pyrr)_2^{2+}$, (b) C_6-$(C_1pyrr)_2^{2+}$, (c) $C_{1O1}C_1pyrr^+$, and (d) $C_3C_1pyrr^+$ at the 0.02 e $bohr^{-3}$ isosurfaces.

Data availability

The data supporting this article (tables of physical properties, structures of the ionic species optimized by DFT calcuations, DSC curves, theoretical electrochemical stabilities, and atomic coordinates of the calculated ionic species) have been included as part of the ESI.†